Journal of
Materials Chemistry B

Accepted Manuscript

This article can be cited before page numbers have been issued, to do this please use: Y. Wang, X. Hu, J. Dai, J. Wang, Y. Tan, X. Yang, S. Yang, Q. Yuan and Y. Zhang, *J. Mater. Chem. B*, 2017, DOI: 10.1039/C7TB01515A.

This is an Accepted Manuscript, which has been through the Royal Society of Chemistry peer review process and has been accepted for publication.

Accepted Manuscripts are published online shortly after acceptance, before technical editing, formatting and proof reading. Using this free service, authors can make their results available to the community, in citable form, before we publish the edited article. We will replace this Accepted Manuscript with the edited and formatted Advance Article as soon as it is available.

You can find more information about Accepted Manuscripts in the author guidelines.

Please note that technical editing may introduce minor changes to the text and/or graphics, which may alter content. The journal's standard Terms & Conditions and the ethical guidelines, outlined in our author and reviewer resource centre, still apply. In no event shall the Royal Society of Chemistry be held responsible for any errors or omissions in this Accepted Manuscript or any consequences arising from the use of any information it contains.

ROYAL SOCIETY OF CHEMISTRY

rsc.li/materials-b

Journal of Materials Chemistry B
View Article Online
DOI: 10.1039/C7TB01515A
Materials for Biology and Medicine

Full paper submission

Journal of Materials Chemistry B is a weekly journal in the materials field. The journal is interdisciplinary, publishing work of international significance on all aspects of materials chemistry related to biology and medicine. Articles cover the fabrication, properties and applications of materials.

2015 Impact Factor of *Journal of Materials Chemistry B*: **4.872**
For more information go to www.rsc.org/materialsB

The following paper has been submitted to *Journal of Materials Chemistry B* for consideration as a **Full paper**.

The Editorial Board stress a **very high quality and novelty** standard is needed for acceptance.

Journal of Materials Chemistry B wishes to publish original research that demonstrates significant **novelty and advance**, either in the chemistry used to produce materials or in the properties/applications of the materials produced. Work submitted that is outside of these criteria will not usually be considered for publication. The materials should also be related to the theme of materials for biology and medicine.

We ask referees to examine manuscripts very carefully, and recommend rejection of articles which do not meet our high novelty, quality and impact expectations. Please note that **the rejection rate for JMCB is currently ~80%** of submitted manuscripts. **Routine or incremental** work, however competently researched and reported, should not be recommended for publication if it does not meet our expectations with regard to novelty and impact.

It is the responsibility of authors to provide fully convincing evidence for the homogeneity and identity of all compounds they claim as new. Evidence of both purity and identity is required to establish that the properties and constants reported are those of the compound with the new structure claimed.

Thank you for your effort in reviewing this submission. It is only through the continued service of referees that we can maintain both the high quality of the publication and the rapid response times to authors. We would greatly appreciate if you could review this paper in **two weeks**. Please let us know if that will not be possible.

Once again, we appreciate your time in serving as a reviewer. To acknowledge this, the Royal Society of Chemistry offers a **25% discount** on its books: http://www.rsc.org/Shop/books/discounts.asp. Please also consider submitting your next manuscript to *Journal of Materials Chemistry B*.

Best wishes,

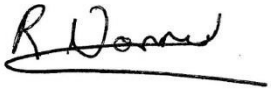

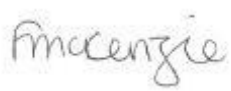

Miss Ruth Norris
Managing Editor, *Journal of Materials Chemistry B*

Dr Fiona McKenzie
Executive Editor, *Journal of Materials Chemistry B*

View Article Online
DOI: 10.1039/C7TB01515A

Journal Name

ARTICLE

A 3D graphene coated bioglass scaffold for bone defect therapy based on molecular targeting approach

Received 00th January 20xx,
Accepted 00th January 20xx

DOI: 10.1039/x0xx00000x

www.rsc.org/

Yulan Wang,[ac+] Xiaoxia Hu,[b+] Jing Dai,[a] Jie Wang,[b] Yaning Tan,[b] Xiangdong Yang,[b] Shuang Yang,[a] Quan Yuan*[b] and Yufeng Zhang*[ac]

Development of a cell-free scaffold with excellent mechanical properties and osteoconductivity is a significant need for bone regeneration. Herein, a reduced graphene oxide (rGO) functionalized hierarchical macro-mesoporous bioactive glass scaffold integrated with osteoblast-specific aptamer is rationally designed to recruit and induce rapid differentiation of osteoblasts for bone regeneration. The scaffold exhibits a macroporous structure with fully interconnected open pores and shows excellent mechanical properties with Young's modulus of ~80 KPa, which provides a strong scaffold to support the growth of osteoblasts and bone tissue regeneration. Furthermore, the scaffold displays good performance in accelerating osteoblast differentiation and promoting newly bone formation. The osteoblast recruitment is achieved since the osteoblast-specific aptamer can specifically target osteoblasts with strong binding affinity. Micro-computed tomography and histological tests confirmed that the large bone defects fully heal with new plate-like-pattern bone appearing both peripherally and centrally, suggesting the outstanding bone regeneration performance of this cell-free and graphene functionalized scaffold. Considering the promising bioapplications of the graphene functionalized bioactive glass scaffold with osteoblast recruitment capacity, our strategy paves a way for the design of new bioactive functional materials for tissue regeneration and shows attractive prospects in targeted therapy.

Introduction

Reconstruction of large bone defects resulting from trauma, infection and tumors remains a medical challenge.[1] Concerning the risk of disease transfer, infection and chronic pain associated with autograft, synthetic bone substitute materials that are able to mimic the structural and biological properties of natural bone have been drawing a significant attention for bone regeneration in current clinical treatments.[2, 3] Compared with traditional bone substitutes, tissue engineering approaches aim to aid the regeneration of bone tissue by filling the bone defects with an osteoconductive scaffold loaded with growth factors and osteogenic cells (mesenchymal stem cells/osteoblasts).[4–6] Osteoblasts are cells which originate in the bone marrow and contribute to the production of new bone. They are responsible for bone matrix synthesis and also play a role in subsequent mineralization.[7, 8] However, immune rejection, source limitation, pathogen transmission, and issues with packaging prevent the therapeutic use of cell-loaded scaffolds.[9, 10] Cell-free approaches utilizing a surface functionalized bioactive glass scaffold to induce bone regeneration by endogenous osteoblasts may provide a suitable alternative to improve bone regeneration. For enhancing the efficacy of bone regeneration, synthetic scaffolds need to capture osteoblasts and exhibit sufficient mechanical strength to withstand physiological loading, thereby providing a microenvironment suitable for osteoblasts to proliferate, differentiate and mineralize.[11]

Graphene, the new allotrope of carbon, is defined as a two-dimensional honeycomb lattice composed of monolayer of carbon atoms.[12, 13] Graphene and its derivatives have received tremendous attention in the field of materials science.[14–16] The unique physicochemical and structural properties (e.g., high elasticity, excellent mechanical strength, and large surface area) of graphene make it attractive for application in composite materials.[17] Due to its high Young's modulus (0.5–1 TPa), the incorporation of graphene into brittle materials can surely improve their mechanical properties.[13, 18] It is worth noting that graphene induces no obvious toxic effects *in vivo* and exhibits favorable biocompatibility.[19, 20] Thus, graphene has emerged as an attractive bioactive component of biomaterials for tissue engineering.[21] Furthermore, the ability of graphene to accelerate the osteogenic differentiation of mesenchymal stem cells and osteoblasts, as shown in recent studies,[22] render it attractive for researchers in bone tissue engineering. *In vitro* studies demonstrated that graphene supports the proliferation of mesenchymal stem cells/osteoblasts and accelerates their differentiation into mature osteoblasts.[23, 24] Taking

[a] State Key Laboratory Breeding Base of Basic Science of Stomatology (Hubei-MOST) and Key Laboratory of Oral Biomedicine Ministry of Education, School and Hospital of Stomatology, Wuhan University, China. E-mail: zyf@whu.edu.cn.
[b] Key Laboratory of Analytical Chemistry for Biology and Medicine (Ministry of Education), College of Chemistry and Molecular Sciences, Wuhan University, China. E-mail: yuanquan@whu.edu.cn.
[c] Medical Research Institute, School of Medicine, Wuhan University, China
+ These authors contributed equally to this work.
† Electronic Supplementary Information (ESI) available: Experimental details and supplementary results. See DOI: 10.1039/x0xx00000x

View Article Online
DOI: 10.1039/C7TB01515A

into consideration both its excellent mechanical properties and favorable biocompatibility, graphene is a promising material in combination with synthetic scaffolds to enhance their mechanical strength and improve their bioactivity. In addition, reduced graphene oxide (denoted as rGO), which is usually denominated as chemically modified graphene, is rich in carboxyl groups on its surface.[25] These functional groups provide reactive handles for surface modification to add biochemical functionality, such as recognition of specific targets.[26] Similar to antibodies, aptamers, which are single-stranded DNA/RNA oligonucleotides, function primarily in molecular recognition, and have the capacity to recognize and bind with target molecules with high affinity and specificity.[27] Aptamers have the additional advantages of small size, low production cost, facile chemical modification, low immunogenicity, low batch-to-batch variation, high chemical stability, rapid tissue penetration, and no toxicity. In order to enrich endogenous osteoblasts in the bone defect, an osteoblast-specific aptamer can be immobilized on the bioactive glass scaffold to give it capacity to capture endogenous osteoblasts around the bone defect.

This paper reports the use of rGO for surface coating of hierarchically macro-mesoporous bioactive glass (denoted as MBG) to construct a new three-dimensional bioactive porous scaffold. The raw material, MBG, is a biocompatible bone regeneration scaffold,[28] which is capable of stimulating bone growth by its dissolution products and rapid bonding with the host bone without causing fibrous encapsulation.[29–31] Graphene coating successfully improved the mechanical properties of MBG to support loads experienced by the newly formed bone in large bone defects. This architecture could provide a microenvironment to satisfy the requirements for osteoblasts to proliferate, deposit bone extracelluar matrix and generate new bone formation.

Results and discussion

As shown in Scheme 1a, a MBG scaffold with hierarchically macro-mesoporous structure was first produced by the sol-gel method. Then, it was coated with rGO sheets. Finally, to achieve osteoblast enrichment in scaffolds, the scaffold surface was modified with osteoblast-specific aptamer CH6. This rGO-coated and aptamer-immobilized MBG scaffold (denoted as rGO-MBG-AP) was implanted in the bone defect, and it successfully fulfilled the requirement to capture osteoblasts to the scaffold surface (Scheme 1b). Furthermore, the rGO-coated and aptamer-immobilized MBG (denoted as rGO-MBG-AP) improved the mineralization of osteoblasts, as shown in a study of the interaction between the scaffold and rat femur osteoblasts. Through surface modification by rGO and osteoblast-specific aptamer, the bone substitute scaffold with sufficient mechanical strength displayed specific recognition to recruit osteoblasts, and achieved the integration of osteoblast enrichment, differentiation and bone tissue regeneration. Considering the promising bioapplications of graphene and the specific recognition of an aptamer for its target, our strategy paves the way to design new bioactive functional materials for tissue regeneration and shows attractive application prospects for targeted therapy.

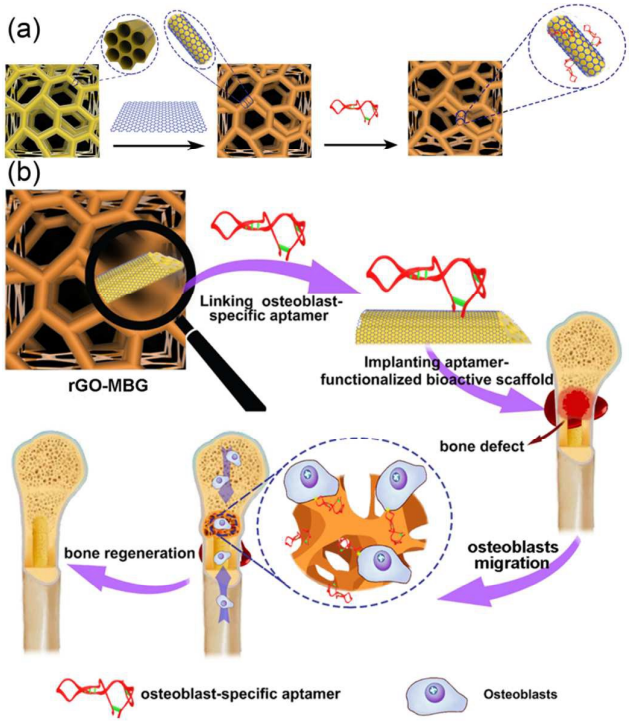

Scheme 1 (a) Overview of rGO-MBG-AP in critical bone defect repair. (b) Schematic diagram of the scaffold construction.

Size and distribution of pores within tissue-engineered scaffolds have an important role in directing cellular behaviour. The morphology of the as-prepared rGO-MBG-AP were investigated by means of scanning electron microscopy (SEM). As shown in Fig. 1a-c, the MBG, rGO-MBG, and rGO-MBG-AP had similar surface topography. As shown in Fig. 1d-1g, EDS analysis of the corresponding areas of MBG, rGO-MBG and rGO-MBG-AP showed that the atomic percent of C was increased with the addition of rGO (MBG: 19.62%, rGO-MBG: 37.87%), suggesting the successful coated of rGO on the surface of MBG. In addition, the amount of P in rGO-MBG and rGO-MBG-AP was calculated to be 0.02% and 0.13%, respectively. This was mainly because of the conjugation of aptamer on the surface of rGO-MBG. What's more, the rGO-MBG-AP exhibited a macroporous structure with fully interconnected open pores in lower magnicification of SEM images (Fig. 1h). The diameters of the macropores ranged from a few hundred micrometers to one millimeter. Such an internected three dimensional pore network is favorable for cell migration, cell proliferation and ECM deposition. In addition, the microstructure of the rGO-MBG-AP was investigated *via* transmission electron microscopy (TEM), as shown in Fig. 1i. The TEM image showed that the typical mesoporous structure of MBG and the flexible rGO sheets were obtained simultaneously. Apparently, the rGO-MBG-AP maintained its ordered mesoporous structure, and the rGO sheets were shown to be well connected with MBG, confirming that the rGO sheets were coated on the MBG surface. The mechanical property of the rGO-MBG-AP was investigated by comparison with MBG (Fig. S7). The rGO-MBG-AP scaffold with the 7 × 7 mm surface

View Article Online
DOI: 10.1039/C7TB01515A

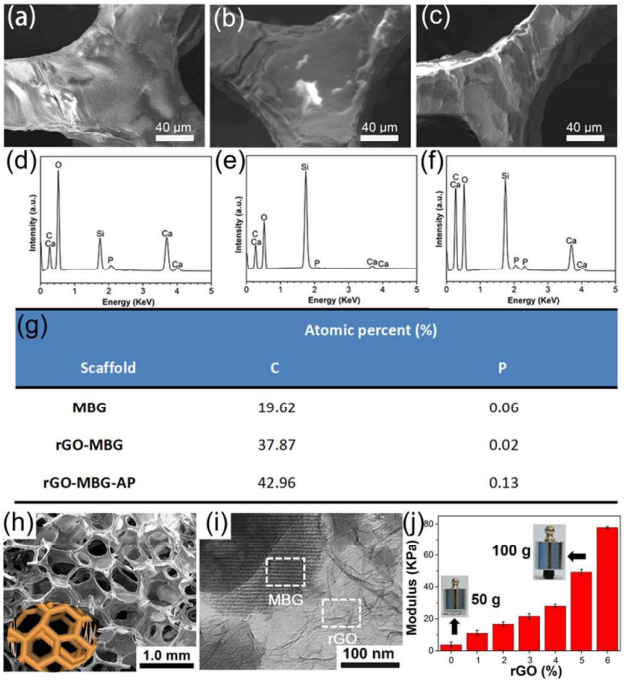

Fig. 1 (a) The highly magnified SEM image of MGB, (b) rGO-MBG, (c) rGO-MBG-AP surfaces. (d) The corresponding EDS spectra of MBG, (e) rGO-MBG, and (f) rGO-MBG-AP. (g) The atomic percent of C and P in the MBG, rGO-MBG, and rGO-MBG-AP scaffolds. (h) Low magnicification of SEM images of rGO-MBG-AP. (i) TEM image of the rGO-MBG-AP, Inset: diagram of rGO-MBG-AP scaffold. (j) Young's Modulus of the MBG and MBG with different compositions of rGO. Inset: photographs of MBG and rGO-MBG-AP withstood 50 grams and 100 grams, respectively.

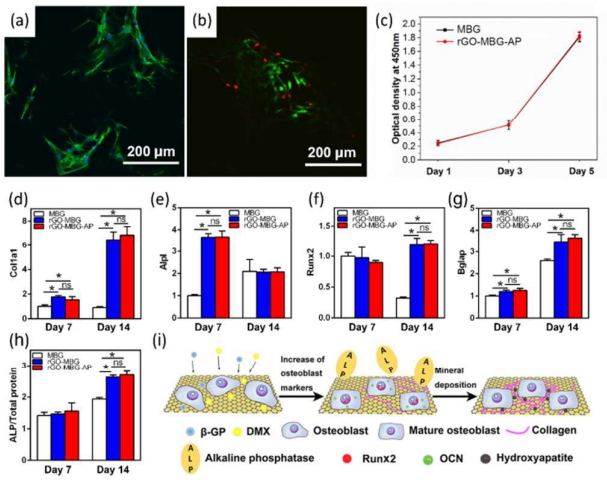

Fig. 2 (a) Confocal microscope images of dead/live cell staining in the rGO-MBG-AP scaffold. (b) Confocal microscope images of the cell morphology in rGO-MBG-AP scaffold. (c) The proliferation of rOBs in rGO-MBG-AP scaffolds. The expression of (d) Col1a, (e) ALP, (f) Runx2, and (g) Bglap in rOBs on the MBG, rGO-MBG and rGO-MBG-AP scaffolds at days 7 and 14. (h) ALP activity of rOBs cultured in the MBG, rGO-MBG and rGO-MBG-AP scaffolds at days 7 and 14. (i) Illustration of osteoblast differentiation accelerated by rGO. All data represent the mean values ± standard deviation (*$p < 0.05$).

area can withstand the wight of 100 g without collapsing, while the MBG with the same surface area collapsed under 50 grams. Thus, the rGO-MBG-AP exhibited superior mechanical properties compared with MBG, demonstrating that graphene plays an important role in enhancing the mechanical properties of rGO-MBG-AP. Furthermore, the compressive strength of rGO-MBG-AP containing different amounts of rGO was measured (Fig. 1j and Fig. S8). The compressive Young's modulus of the rGO-MBG-AP was ~80 KPa, while the MBG without rGO coating was ~2 KPa. In addition, the compressive Young's modulus of the rGO-MBG-AP was significantly enhanced as the mass fraction of rGO increased, thus providing a stronger scaffold to support the growth of recruited osteoblasts and the newly formed bone tissue.

The cytotoxicity of the scaffold *in vitro* was visualized using a fluorescent live/dead assay. Live cells were stained green and appeared to adhere well on the scaffold, while dead cells were stained red and rounded. Little red cells were found in rGO-MBG-AP 3 days after seeding (Fig. 2a). Quantitative analysis based on the dead/live staining further verified the high survival rate of osteoblasts in the scaffolds (Fig. S10). Since cell morphology alteration is the first and most readily noticeable effect following exposure of cells to toxic materials,[32] the morphology of cells in the rGO-MBG-AP was then observed. Phalloidine staining showed that cells had a osteoblast-like morphology (polygonal or spindle cells) with good attachment to the rGO-MBG-AP surface (Fig. 2b), verifying that the rGO-MBG-AP has little influence on the morphology alteration of osteoblasts. The proliferative activity of cells seeded in the rGO-MBG-AP scaffold was investigated at 1, 3 and 5 days. The number of cells increased as time progressed (Fig. 2c), suggesting that the cells maintained good proliferative activity after seeding in the rGO-MBG-AP.

It has been demonstrated that graphene can accelerate the osteogenic differentiation of mesenchymal stem cells and osteoblasts.[24] Therefore, realtime PCR was performed on rat osteoblasts (rOBs) in the scaffolds to investigate the osteoblast differentiation in the rGO-MBG-AP scaffold. The total RNA of rOBs in the scaffolds after 7 and 14 days osteogenic induction was extracted to evaluate the mRNA experession level of four osteoblast markers, collagen type I alpha 1 (Col1a1, an important component of bone extracelluar matrix), alkaline phosphatase (ALP, the enzyme playing an essential role in bone mineralization), runt related transcription factor 2 (Runx2, an essential protein for osteoblastic differentiation and skeletal morphogenesis) and bone gamma-carboxyglutamate protein (Bglap, a protein function in bone remodeling).[33] As shown in Fig. 2d-2g, Col1a1, ALP, Runx2 and Bglap were significantly upregulated in the rGO-MBG-AP group at different levels when compared with those in MBG group, demonstrating that rGO-MBG-AP scaffolds can stimulate bone-related gene expression of rOBs. It is commonly agreed that the *in*

View Article Online
DOI: 10.1039/C7TB01515A

vivo bone-forming bioactivity is related to the apatite layer formation,[34] thus the *in vitro* assessment of bone-forming bioactivity was carried out by soaking rGO-MBG-AP in simulated body fluid (SBF) and then monitoring apatite formation (Fig. S11). SEM images (Fig. S12) revealed that the surface of rGO-MBG-AP was fully covered by an apatite-like phase composed of rod-like particles after soaking in SBF for 7 days, and the amount of hydroxyapatite (HA) nanocrystals increased as the soaking time increased from 1 to 7 days. The X-ray diffraction (XRD) pattern of rGO-MBG-AP showed the characteristic peaks of the crystalline HA phase after immersing in SBF for 7 days (Fig. S14). It was observed that more apatite microparticles were present on the rGO-MBG-AP surface compared to the amount on the MBG scaffold surface after immersion in SBF for 7 days (Fig. S15), demonstrating that the rGO-MBG-AP scaffold has better *in vivo* bone-forming bioactivity than MBG. The ALP activity of rOBs in the scaffolds after culture in osteogenic medium was illustrated in Fig. 2h, and the rGO-MBG-AP scaffold showed higher ALP/Total protein ratio than that of MBG scaffold at days 7 and 14. Since ALP plays an important role in calcification during bone formation, our results indicate that the rGO-MBG-AP scaffold has better performance in inducing the calcification of rOBs. Recent studies have shown that rGO can act as a preconcentration platform for dexamethasone and β-glycerolphosphate,[23] and the increase in concentration of dexamethasone and β-glycerolphosphate was reported to improve the expression levels of proteins and enzymes needed in osteoblast differentiation.[35] In this case, it is speculated that dexamethasone and β-glycerolphosphate were first preconcentrated in the rGO-MBG-AP scaffold (Fig. 2i, left), and then the increased local osteogenic inducers functioned on immature osteoblasts to increase the osteoblast markers (Fig. 2i, middle). Furthermore,

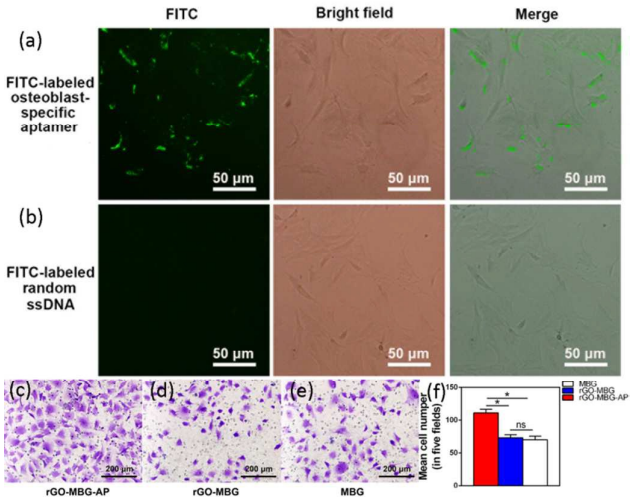

Fig. 3 Fluorescent images of the binding of rOBs with (a) FITC-labeled osteoblast-specific aptamer and (b) FITC-labeled random ssDNA. Light microscopy images of the transwell assay of rOBs toward (c) rGO-MBG-AP, (d) rGO-MBG, and (e) MBG scaffolds. (f) Cell number of the transwell assay of rOBs toward rGO-MBG-AP, rGO-MBG, and MBG scaffolds. All data represent the mean values ± standard deviation (*$p < 0.05$).

more hydroxyapatite was deposited on the rGO-MBG-AP scaffold as illustrated in the right part of Fig. 2i, thus providing a better osteogenic microenvironment for new bone formation. These results demonstrated that the rGO-MBG-AP holds great promise in accelerating osteoblast differentiation and mineral deposition in vitro and such bioactivity studies verified the great osteoconductivity of this scaffold.

Because an osteoblast-specific aptamer named as CH6[36] was conjugated to the rGO-MBG scaffold for faster recruiting of the immature osteoblasts, fluorescent microscopy and flow cytometry were used to verify the specific binding of CH6 aptamer and osteoblasts. As shown in Fig. 3a, the cells treated with this osteoblast-specific aptamer CH6 showed strong fluorescence. In comparison, the cells treated with FITC-labeled random ssDNA showed much less binding to osteoblasts (Fig. 3b), confirming the targeting role and high affinity of CH6 aptamer. The targeting specificity of CH6 aptamer toward rOBs was also confirmed by flow cytometry (Fig. S16). When CH6 aptamer was incubated with rOBs at 37 °C, strong fluorescence intensity was observed, demonstrating that CH6 aptamer can bind to rOBs with high binding affinity. In contrast, when incubated with fibroblasts, no fluorescence was observed. Therefore, CH6 aptamer exhibited stronger specific binding affinity for rOBs compared to random cells. What's more, when CH6 aptamer was cultured with whole bone marrow, a slight fluorescence enhancement was observed compared to the fibroblasts group, indicating that CH6 aptamer can specifically bind with rOBs from whole bone marrow. It is widely accepted that recruitment of osteoblasts to the defect site is essential in the regeneration of bone defect, and that lack of osteoblast recruitment leads to poor healing.[37–39] Thus, realization of osteoblast recruitment is a promising strategy to improve bone formation in bone defects. In this case, rOBs cultured from femoral cancellous bone were utilized to test the specific aptamer binding, and the rOBs recruitment ability of rGO-MBG-AP was performed by the transwell assay. As shown in Fig. 3c, the number of cells which migrated to the rGO-MBG-AP scaffold was much higher than the number in the rGO-MBG scaffold (Fig. 3d) and MBG (Fig. 3e). The statistical data showed that there were 108 ± 6 rOBs in the rGO-MBG-AP scaffold, while only 74 ± 6 rOBs were in the rGO-MBG scaffold (Fig. 3f). Therefore, the addition of osteoblast specific aptamer has significantly improved the osteoblast migration toward the scaffold ($p < 0.05$), verifying that the rGO-MBG-AP scaffold possesses an outstanding capability for osteoblasts recruitment.

In vivo studies were carried out to evaluate the bone regeneration ability of this scaffold. Sprague Dawley rats were used to investigate the bone regeneration abilities of rGO-MBG-AP scaffolds (Fig. S17). A skin incision was made in the distal femoral epiphysis and blunt dissection was performed on the muscles to expose the femoral condyle. Then, an anteroposterior bicortical channel with a diameter of 2.8 mm was created in the rat femur perpendicular to the shaft axis, and the cancellous trabecular bone was destroyed using a trephine bur (left side of Fig. S17). The scaffolds were perpared to fit the defect size, and the macromorphology of the bulk material is shown in the middle of Fig. S17. After that, the drilled defects were rinsed by injection with normal saline to remove bone fragments from the cavity. The

View Article Online
DOI: 10.1039/C7TB01515A

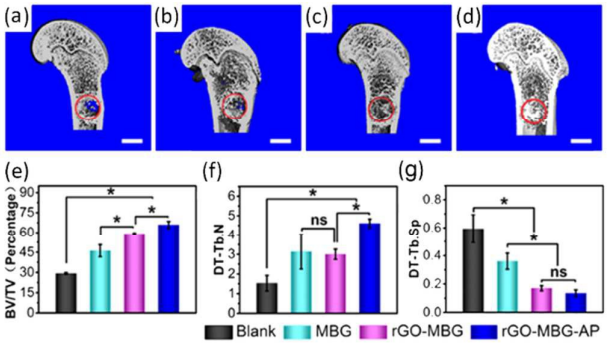

Fig. 4 (a) μ-CT 3D reconstruction of the femur defects treated with nothing, (b) MBG, (c) rGO-MBG and (d) rGO-MBG-AP in the eighth week. The red circle presents the bone defect. Scale bars, 2 mm. (e) Quantification of bone volume density (BV/TV, bone volume/tissue volume). (f) Quantification of trabecular number (Tb. N). (g) Quantification of trabecular density (Tb. Sp, trabecular separation). All data represent the mean values ± standard deviation (N = 3, *p < 0.05).

scaffold was then carefully implanted into the bone defects, as shown in the right side of Fig. S17. The rats were bred for 8 weeks after implantation for new bone formation. Then the femurs were removed from the rats and examined by micro-computed tomography (μ-CT) to assess new bone formation. The bone defects treated with MBG and nothing were applied as control groups. After three dimensional (3D) reconstruction, μ-CT images and micro-architectural parameters were collected to show the morphology of newly regenerated bone and to quantify the mineralization of new bone formation within defects. The 3D reconstruction images show obvious differences in the defects treated with rGO-MBG-AP, rGO-MBG, MBG, and nothing. After 8 weeks healing, there was minimal new bone formation within the defect treated with nothing and the bone defect remained almost empty, indicating that the bone defect could not be regenerated by self-healing (Fig. 4a). As shown in Fig. 4b, when the bone defect was treated with MBG, there was newly regenerated bone around the defect border. However, the center of the defect still remained empty. It is obvious that the defects treated with MBG showed slightly increased new bone volume compared to the untreated defect. As shown in Fig. 4c, when the defect was treated with rGO-MBG, there was newly regenerated bone around the bone defect. Compared with the defect treated with MBG, the defect showed slight increased new bone formation in the bone defect, indicating that rGO possesses a potential for improving bone regeneration. Significantly, the bone defect treated with rGO-MBG-AP was found to fully heal with new plate-like-pattern bone appearing both peripherally and centrally, as shown in Fig. 4d. The amount of newly formed bone in the rGO-MBG-AP goup was significantly higher than that in either the MBG group or rGO-MBG group. These results demonstrated that rGO-MBG-AP exhibited best performance in bone regeneration, largely due to the osteogenic induction of rGO and the high affinity of osteoblast-specific aptamer with rOBs. In accordance with the image observation, 3D micro-architectural parameters, including the ratio of bone volume/tissue volume (BV/TV), trabecular number (Tb. N), and trabecular separation (Tb. Sp), were assessed as quantitative indicators of new bone formation. BV/TV represents the amount of trabecular bone within the bone defect area and is evidence of new bone formation.[40] The BV/TV of the rGO-MBG-AP group was the highest among four groups, indicating that the amount of trabecular bone in this group was maximum (Fig. 4e). Tb. N is an indicator of bone density.[41] As shown in Fig. 4f, the rGO-MBG-AP group exhibited the highest Tb. N, together with the highest trabecular bone amount shown in Fig. 4e, demonstrating that the rGO-MBG-AP group has the highest bone density. Tb. Sp represents the spacing between bone trabecula and is another indicator of bone density.[41] The trabecular microstructure of rGO-MBG-AP was found to be the best, because the Tb. Sp of this scaffold is the lowest among all groups in Fig. 4g, indicating a much more thickened regrown cancellous bone compared to other groups.

Histomorphological analysis by hematoxylin & eosin (H&E) staining was carried out to evaluate bone regeneration within the defect site. The new bone formation induced by the defect treated with rGO-MBG-AP was confirmed by the histological evaluation after 4 and 8 weeks implantation. In the histological image acquired in the fourth week, no appreciable bone formation was observed in the blank group treated with nothing (Fig. 5a). Moreover, the defect center of the blank group was filled with bone marrow-like tissue instead of new bone in the eighth week, demonstrating that the self-healing ability of bone defect is not sufficient (Fig. 5b). When the bone defect was treated with MBG for 4 weeks, loose connective fibrous tissues were largely populated in the defect site, and no obvious new bone formation was obtained (Fig. 5c). Compared with the results in the fourth week, new bone tissues were found to be dispersed and not connected with each other aftter treatment with MBG for 8 weeks (Fig. 5d). Meanwhile, the MBG scaffold failed to maintain its structure and degraded into small pieces due to its brittleness and fragility. Thus, the poor mechanical strength of MBG cannot provide a stable support for new bone regeneration. As for the rGO-MBG group, newly formed bone tissue can be observed in the defect area in the fourth week (Fig. 5e). An increasing volume of new bone tissues was observed after eight weeks healing, and a number of well mineralized bone tissues were formed (Fig. 5f). Newly formed bone tissues were much more arranged than those in the MBG group and lined beside the rGO-MBG surface. Therefore, the addition of rGO significantly improved the mechanical property of the scaffold to support the growth of newly regenerated bone and had a good performance in improving the bone regeneration. Notably, when the bone defect was treated with rGO-MBG-AP, a large scale of bone tissue and mineralized bone matrix deposition were displayed in the fourth week as illustrated in Fig. 5g. After 8 weeks implantation, the H&E staining of the group treated with rGO-MBG-AP showed that the defect was mainly filled with well-arranged new bone tissue and mineralized bone matrix deposition (Fig. 5h). These newly formed bone tissues directly integrated with the rGO-MBG-AP scaffolds (Fig. 5h, blue stars). Compared with the defect treated with MBG and rGO-MBG groups, much more new bone tissue along the rGO-MBG-AP interface was observed. In addition, an increased amount of osteoblastic cells and matrix were obtained in the defect treated with rGO-MBG-AP. The maximum new bone observed beside the

View Article Online
DOI: 10.1039/C7TB01515A

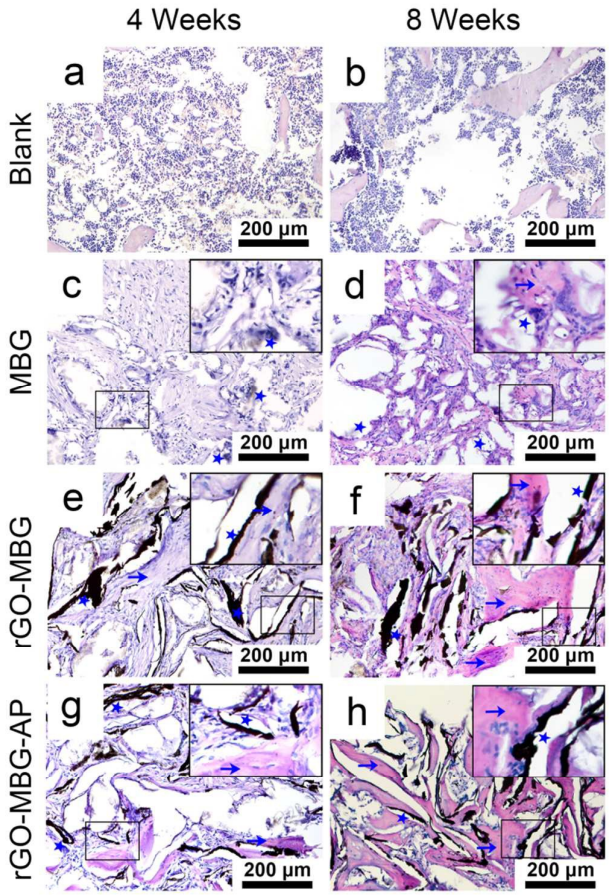

Fig. 5 Histological analysis of bone defects at different time points. (a) Blank group (defect treated with nothing) in the fourth week and (b) eighth week. (c) MBG in the fourth week and (d) eighth week. (e) rGO-MBG group in the fourth week and (f) eighth week. (g) rGO-MBG-AP in the fourth week and (h) eighth week. The box on the right top gives magnification of local details. Arrows: new generated bone tissue. Stars: treated scaffolds.

rGO-MBG-AP interface suggested that both rGO and osteoblast specific aptamer significantly improved the new bone regeneration. As a result, the rGO-MBG-AP is promising for accelerating the new bone formation. The immunohistochemical staining of Col1a (Fig. S18) showed that the rGO-MBG-AP was surrounded by abundant amounts of Col1a in the fourth and eighth week. In contrast, minimal Colla was detected by immunohistochemical staining when the defect was treated with MBG. As Col1a is an important component of the bone extracelluar matrix, this result comfirmed that rGO-MBG-AP has the best ability for bone matrix deposition among all groups. These histological analyses further verified the results obtained by μ-CT that rGO-MBG-AP showed the best bone regeneration capacity.

Conclusions

In this work, a graphene functionalized 3D bioactive glass scaffold with ability to recruit osteoblasts was constructed for regeneration of bone defects. The osteogenic differentiation of the osteoblasts was efficiently upregulated through the osteogenic inducer preconcentration of the rGO coating in the rGO-MBG-AP scaffolds. The mechanical strength of the scaffold has been significantly improved through rGO coating, thus providing a strong scaffold to support the growth of osteoblasts. Since the scaffold exhibited no negative effect on cell attachment, morphology and proliferation, it appears to be attractive for bioapplication. The osteoblast-specific aptamers were effectively immobilized on the surface of the 3D hierarchical structure, and osteoblast recuitment was achieved since the aptamers can specifically target osteoblast cells with high affinity. The rGO-MBG-AP scaffold exhibited outstanding results for bone regeneration in critical femur bone defects through recruiting and osteogenic induction of osteoblasts. To conclude, by applying rGO and aptamer in the 3D structure of MBG, increased mechanical stability and better osteogenic capacity were successfully obtained. This strategy can serve as an effective approach for cell recruitment in tissue engineering and is anticipated to find broad application in regenerating new tissues and organs.

Acknowledgements

This work was supported by the National Natural Science Foundation of China (81271108, 81570954, 21675120 and 21422105), the Fundamental Research Funds for the Central Universities (410500041), and Ten Thousand Talents Program for Young Talents (to Quan Yuan). Q. Yuan thanks the large-scale instrument and equipment sharing foundation of Wuhan University. The authors declare no competing financial interest.

Notes and references

1 G. Calori, E. Mazza, M. Colombo, C. Ripamonti, *Injury 2011,* **42**, S56.
2 Y. Xiao, H. Haase, W. G. Young, M. Bartold, *Cell Transplant.* **2004**, *13*, 15.
3 E. Gruskin, B. A. Doll, F. W. Futrell, J. P. Schmitz, J. O. Hollinger, *Adv. Drug. Deliver. Rev. 2012*, **64**, 1063.
4 V. A. Siclari, J. Zhu, K. Akiyama, F. Liu, X. Zhang, A. Chandra, H. D. Nah, S. Shi, L. Qin, *Bone 2013*, **53**, 575.
5 S. Font Tellado, E. R. Balmayor, M. Van Griensven, *Adv. Drug. Deliver. Rev. 2015*, **94**, 126.
6 W. L. Grayson, B. A. Bunnell, E. Martin, T. Frazier, B. P. Hung, J. M. Gimble, *Nat. Rev. Endocrinol. 2015*, **11**, 140.
7 G. Karsenty, *Annu. Rev. Genomics. Hum. Genet. 2008*, **9**, 183.
8 M. B. Greenblatt, J. H. Shim, L. H. Glimcher, *Annu. Rev. Cell. Dev. Biol. 2013*, **29**, 63.
9 T. H. Qazi, D. J. Mooney, M. Pumberger, S. Geißler, G. N. Duda, *Biomaterials 2015*, **53**, 502.
10 D. J. Prockop, *Mol. Ther. 2009*, **17**, 939.
11 Q. Fu, E. Saiz, A. P. Tomsia, *Adv. Funct. Mater. 2011*, **21**, 1058.
12 A. K. Geim, K. S. Novoselov, *Nat. Mater. 2007*, **6**, 183.
13 Y. Chen, C. Tan, H. Zhang, L. Wang, *Chem. Soc. Rev. 2015*, **44**, 2681.
14 Y. Chen, C. L. Tan, H. Zhang, L. Z. Wang, *Chem. Soc. Rev. 2015*, **44**, 2681.
15 Y. Oh, M. F. Islam, *ACS Nano 2015*, **9**, 4103.
16 Y. F. Wang, S. Chen, L. Qiu, K. Wang, H. Wang, G. P. Simon, D. Li, *Adv. Funct. Mater. 2015*, **25**, 126.

View Article Online
DOI: 10.1039/C7TB01515A

17 M. Mehrali, E. Moghaddam, S. F. S. Shirazi, S. Baradaran, M. Mehrali, S. T. Latibari, H. S. C. Metselaar, N. A. Kadri, K. Zandi, N. A.A. Osman, *ACS Appl. Mater. Interfaces 2014*, **6**, 3947.
18 I. W. Frank, D. M. Tanenbaum, A. M. van der Zande, P. L. McEuen, *J. Vac. Sci. Technol., B 2007*, **25**, 2558.
19 J. T. Robinson, S. M. Tabakman, Y. Y. Liang, H. L. Wang, H. S. Casalongue, D. Vinh, H. J. Dai, *J. Am. Chem. Soc. 2011*, **133**, 6825
20 G. S. Hong, S. Diao, A. L. Antaris, H. J. Dai, *Chem. Rev. 2015*, **115**, 10816.
21 K. Kostarelos, K. S. Novoselov, *Science 2014*, **344**, 261.
22 T. R. Nayak, H. Andersen, V.S. Makam, c.Khaw, S. Bae, X. F. Xu, P. L. R. Ee, J. H. Ahn, B. H. Hong, G. Pastorin, B. Özyilmaz, *ACS Nano 2011*, **5**, 4670.
23 W. C. Lee, C. H. Y. Lim, H. Shi, L. A. Tang, Y. Wang, C. T. Lim, K. P. Loh, *ACS Nano 2011*, **5**, 7334.
24 Y. C. Shin, J. H. Lee, O. S. Jin, S. H. Kang, S. W. Hong, B. Kim, J.C. Park, D.W. Han, *Carbon 2015*, **95**, 1051.
25 C. Li, G. Q. Shi, *Adv. Mater. 2014*, **26**, 3992.
26 H. Liang, X. B. Zhang, Y. Lv, L. Gong, R. Wang, X. Zhu, R. Yang, W. Tan, *Acc. Chem. Res. 2014*, **47**, 1891.
27 X. Fang, W. Tan, *Acc. Chem. Res. 2010*, **43**, 48.
28 X. Yan, C. Yu, X. Zhou, J. Tang, D. Zhao, *Angew. Chem. Int. Ed. 2004*, **43**, 5980; *Angew. Chem. 2004*, **116**, 6106.
29 C. Wu, L. Xia, P. Han, L. Mao, J. Wang, D. Zhai, B. Fang, J. Chang, Y. Xiao, *ACS Appl. Mater. Interfaces 2016*, **8**, 11342.
30 Y. Zhang, L. Xia, D. Zhai, M. Shi, Y. Luo, C. Feng, B. Fang, J. Yin, J. Chang, C. Wu, *Nanoscale 2015*, **7**, 19207.
31 C. Wu, J. Chang, *J. Control. Release. 2014*, **193**, 282.
32 J. Lee, G. D. Lilly, R. C. Doty, P. Podsiadlo, N. A. Kotov, *Small 2009*, **5**, 1213.
33 Y. Zhang, L. Wei, J. Chang, R. J. Miron, B. Shi, S. Yi, C. Wu, *J. Mater. Chem. B 2013*, **1**, 5711.
34 Q. H. Shi, J. F.Wang, J. P. Zhang, J. Fan, G. D. Stucky, *Adv. Mater. 2006*, **18**, 1038.
35 L. Meinel, R. Fajardo, S. Hofmann, R. Langer, J. Chen, B. Snyder, G. Vunjak-Novakovic, D. Kaplan, *Bone 2005*, **37**, 688.
36 C. Liang, B. Guo, H. Wu, N. Shao, D. Li, J. Liu, L. Dang, C. Wang, H. Li, S. Li, W. K. Lau, Y. Cao, Z. Yang, C. Lu, X. He, D. W. T. Au, X. Pan, B.-T. Zhang, C. Lu, H. Zhang, K. Yue, A. Qian, P. Shang, J. Xu, L. Xiao, Z. Bian, W. Tan, Z. Liang, F. He, L. Zhang, A. Lu, G. Zhang, *Nat. Med. 2015*, **21**, 288.
37 D. Park, J. A. Spencer, B. I. Koh, T. Kobayashi, J. Fujisaki, T. L. Clemens, C. P. Lin, H. M. Kronenberg, D. T. Scadden, *Stem cell 2012*, **10**, 259.
38 C. Maes, T. Kobayashi, M. K. Selig, S. Torrekens, S. I. Roth, S. Mackem, G. Carmeliet, H. M. Kronenberg, *Dev. Cell 2010,* **19**, 329.
39 Y. Wang, J. Zhu, H. F. DeLuca, *J. Bone. Mine. Res. 2014*, **29**, 685.
40 H. Scherf, J. Wahl, J. J. Hublin, K. Harvati, *Am. J. Phys. Anthropol. 2016*, **159**, 106.
41 E. Legrand, D. Chappard, C. Pascaretti, M. Duquenne, S. Krebs, V. Rohmer, M. F. Basle, M. Audran, *J. Bone. Miner. Res. 2000,* **15**, 13.